# TURBULENCE ENHANCEMENT BY FORCED SHOCK MOTION IN SHOCK-WAVE/TURBULENT BOUNDARY LAYER INTERACTION

**S. Hickel, O.C. Petrache and N.A. Adams**

Institute of Aerodynamics and Fluidmechanics
Technische Universität München
Boltzmannstrasse 15, 85747 Garching, Germany
Email: sh@tum.de

## ABSTRACT

We present Implicit Large-Eddy Simulations of a shock-wave/turbulent boundary layer interaction (SWTBLI) at $Ma = 2.25$ and $Re_\delta = 51,552$ with and without localized heat addition. The flow is complex and involves boundary layer separation under the adverse pressure gradient imposed by the shock, turbulence amplification across the interaction and low frequency oscillation of the reflected shock. For an entropy spot generated ahead of the shock, baroclinic vorticity production occurs when the resulting density peak passes the shock. The objective of the present study is to analyze the shock-separation interaction and turbulence structure of such a configuration. The effect of the addition of an entropy spot to the flow field is assessed in terms of turbulence amplification and turbulence mass flux.

## INTRODUCTION

The SCRamjet is a flight propulsion engine meant to operate at hypersonic speeds. At flight Mach numbers $Ma > 5$, the flow goes initially through forebody compression and, as it progresses through the isolator and entries into the combustion chamber, is further decelerated through a shock train. Combustion usually takes place at around $Ma = 2$. Such speeds result in a flow residence time on the order of milliseconds. In order to achieve the desired combustion efficiency, a very good fuel/air mixing rate is required. Classically, the fuel-injector type (strut, ramp or wall injector) is primarily determining the mixing process. Another, less-investigated way to improve the fuel-to-air mixing is to exploit the presence of the aforementioned shock train. In the SCRamjet isolator and combustion chamber, oblique shocks propagate by reflection at the wall, where they impinge on turbulent boundary layers. Several reports on reflected shock unsteadiness in shock-wave/turbulent boundary layer interaction (SWTBLI) point to a low-frequency mechanism of the reflected shockwave (Dussauge et al., 2006; Pirozzoli et al., 2008; Priebe et al., 2009; Touber and Sandham, 2008; Wu and Martin, 2008). In addition to this, studies showed (Fabre et al., 2001; Hussaini and Erlebacher, 1999) that convecting local variations of temperature through a shock generates an acoustic wave and vorticity. In the SCRamjet frame local variations of temperature can be interpreted as hotter regions, where fuel has burned, or colder regions rich in unburnt fuel. These spots are convected through oblique shocks with the freestream velocity. Our investigation evolves around the benefit fuel/air mixing can obtain from reflected shock oscillation mechanism and convection of entropy spots through an oblique shock. This paper is organized as follows: introduction; description of the numerical method; boundary conditions and computational setup; validation of the turbulence model we used in our simulations; in the fifth part we focus on SWTBLI simulations; the last part is reserved for discussing the influence of entropy spots (ES) convection through the aforementioned flow case.

## NUMERICAL METHOD

The governing equations in our simulations are the fully compressible three-dimensional Navier-Stokes equations written in conservative form

$$\partial_t U + \nabla \cdot F(U) + \nabla \cdot D(U) = 0, \tag{1}$$

where U = [$\rho$, $\rho$u, $\rho$v, $\rho$w, E] is the solution vector containing the conserved variables: density ($\rho$), momentum ($\rho$u, $\rho$v, $\rho$w) and total energy ($E$). We distinguish between the convective fluxes, $F$, and the diffusive fluxes, $D$. The flow non-dimensional parameters are the Mach number, $Ma$, Reynolds number, $Re$, and Prandtl number, $Pr$. To close to system of equations we use the perfect-gas equation of state $\rho T = \gamma Ma^2 p$ and a powerlaw for the viscosity $\mu = \mu_\infty (T/T_\infty)^{0.75}$. Our flow solver INCA is a finite volume method for Large Eddy Simulation (LES). For phenomena involving mechanisms that may invalidate underlying assumptions of classical turbulence models it is necessary to rely on more elaborate approaches such as implicit LES. Implicit LES modeling involves a direct coupling between the truncation error of the numerical scheme and the SGS model. We use the Adaptive Local Deconvolution Method (ALDM; Hickel and Larsson, 2008), which also account for the effects of unresolved subgrid scales, for discretizing the convective fluxes, $F(U)$. For the diffusive fluxes, $D(U)$, we used a $4^{th}$ order centered scheme. Time integration is done with a $3^{rd}$ order explicit Runge-Kutta method.

## COMPUTATIONAL SETUP

When simulating turbulent flows, one of the challenging problems is to generate time-dependent inflow data. For

doing so, there are a few widely used methods: synthetic turbulence approach, digital filter technique and rescaling-recycling technique. For the present simulations of turbulent flows, we use a simplified and general version of the latter, which generates inflow data in a general widely applicable way. Based on the assumption that the boundary layer growth between the inflow and recycling plane is negligible in terms of LES grid resolution, we rescale density and temperature (Eqn. 2 and 3) and then the momentum using Eqn. 4. Index "i" stands for quantity at the inflow plane, "r" represents the recycling station; "$\langle * \rangle$" is used for the time-averaged quantity, while no brackets were used for the instantaneous value of the quantity.

$$\rho_i = \langle \rho \rangle_i + \sqrt{\frac{(\rho'\rho')_i}{(\rho'\rho')_r}} \cdot \left( \rho_r - \langle \rho \rangle_r \right) \tag{2}$$

$$T_i = \langle T \rangle_i + \sqrt{\frac{(T'T')_i}{(T'T')_r}} \cdot \left( T_r - \langle T \rangle_r \right) \tag{3}$$

$$(\rho u)_i = \rho_i \cdot u_i = \rho_i \cdot \left[ \langle u \rangle_i + \sqrt{\frac{(u'u')_i}{(u'u')_r}} \cdot \left( u_r - \langle u \rangle_r \right) \right] \tag{4}$$

The total energy and pressure are then computed from

$$E_i = \frac{1}{\gamma(\gamma-1)\cdot Ma^2} \cdot T_i \cdot \rho_i + e_{kin,i} \tag{5}$$

$$p_i = \frac{1}{\gamma Ma^2} \cdot T_i \rho_i \tag{6}$$

For validating our turbulence model, ALDM, and the inflow data generation method for compressible wall-bounded flows, we first performed a supersonic turbulent boundary layer simulation (TBL). We also ran two simulations with two different grid resolutions for the SWTBLI cases. SWTBLI1 will be referred to as the coarse case, while SWTBLI2 will be the fine case throughout this paper. In all simulations the wall was considered adiabatic. The oblique shock was imposed as a boundary condition on the upper side of the domain, using the Ranquine-Hugoniot jump conditions. In spanwise direction we assumed the flow to be periodic.

In all our simulations we have used Cartesian grids. Details concerning their size and recycling station position ($L_{rec}$) in terms of initial boundary layer thicknesses ($\delta_0$), as well as inflow parameters are presented in Table 1. X-coordinate denotes the streamwise direction, Y is wall-normal and Z is spanwise.

Table 1. Computational domain and inflow data.

| Case | $L_x$x$L_y$x$L_z$ | $L_{rec}$ | $Re_{\delta_0}$ | $\delta_0$ | $Ma$ |
|---|---|---|---|---|---|
| TBL | 45x6x3 | 7 | 13,505 | 1 | 2.0 |
| SWTBLI1 | 49x9x3 | 5.5 | 34,675 | 1 | 2.25 |
| SWTBLI2 | 45x8x6 | 5.5 | 25,602 | 0.738 | 2.25 |

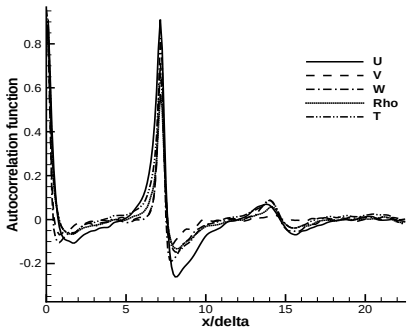


Figure 1. Autocorrelation function for the recycled quantities at $z^+ = 12$.

## FLAT PLATE TURBULENT BOUNDARY LAYER

We performed a TBL simulation to validate our implicit LES model and the rescaling-recycling technique. For comparison we used Direct Numerical Simulation (DNS) data of Pirozzoli et al. (2008). The dimensions of the computational domain in terms of initial boundary layer thicknesses $\delta_0$ are given in Table 1. The grid spacing in viscous wall units is $\Delta x^+ = 32$, $\Delta y^+_{min} \approx 2.4$ and $\Delta z^+ = 16$. The flow field was initialized with a turbulent boundary layer solution generated by a previous temporal simulation. We run the spatial TBL simulation for 225 $\delta_0/u_\infty$ time units, corresponding to five flow-through times at free-stream velocity, before we started recording statistics every 10 time steps (corresponding to a sampling interval of approximately 0.05 $\delta_0/u_\infty$ time units) for 400 $\delta_0/u_\infty$ time units.

The flow needs approximately one recycling length ($7\delta_0$) to adjust to its natural structure. This transient is smaller than in other cases of turbulence inflow data generation methods, such as the Digital Filter technique (Touber and Sandham, 2008), where the transient region can be as big as $15-20\delta_0$. However, if used incautiously, the rescaling-recycling technique has the disadvantage of introducing artificial frequencies proportional to the recycling length in the computational domain. This effect is undesired in the unsteady case of shock-wave/turbulent boundary layer interaction. To overcome this we chose to make the domain in streamwise direction long enough in order to allow for the de-correlation of turbulent quantities. The decay rate of artificial correlations is evaluated by the autocorrelation function in Fig. 1. Close to the wall the autocorrelation is zero after three recycling lengths downstream of the inflow. Artificial correlations are more persistent in the outer part of the boundary layer, but also drop below 0.5 after three recycling lengths, which proves sufficiently fast de-correlation of the turbulent fluctuations. In Fig. 2 we present the comparison between our LES and DNS data of Pirozzoli et al. (2008) at the location with $Re_\delta = 19,089$. Reynolds stresses, normalized with $u_\tau^2 \cdot \sqrt{\rho/\rho_w}$ , as well as the van Driest transformed velocity agree very well with the DNS data. Table 2 summarizes integral parameters for both LES and DNS. We observe an excellent agreement in terms of the friction coefficient $C_f$, displacement thickness $\delta_1$, momentum thickness $\delta_2$ and the shape factors $H = \delta_1/\delta_2$

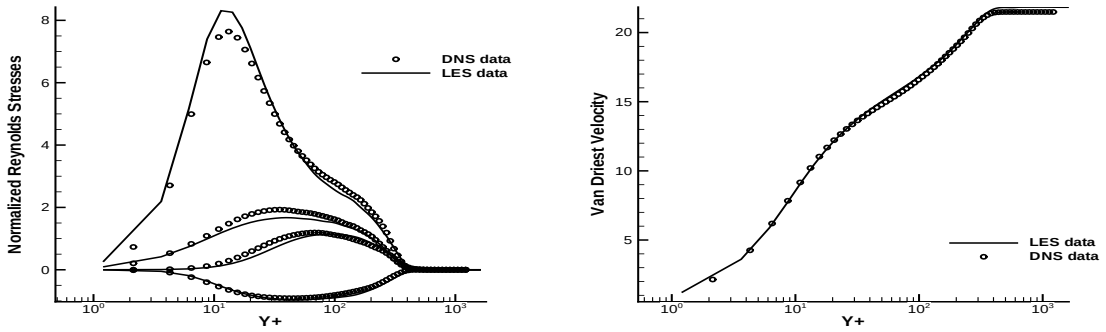


Figure 2. Comparison with DNS data for (a) Reynolds stresses and (b) Van Driest transformed velocity.

and $H_{inc} = \delta_{1,inc}/\delta_{2,inc}$, where $\delta_{1,inc}$ and $\delta_{2,inc}$ are computed with the incompressible formula.

Table 2. Parameters for the turbulent boundary layer.

| Parameter | $C_f$ | $\delta_1/\delta$ | $\delta_2/\delta$ | $H$ | $H_{inc}$ |
|---|---|---|---|---|---|
| LES | 0.00296 | 0.236 | 0.083 | 2.84 | 1.44 |
| DNS | 0.00297 | 0.249 | 0.082 | 3.03 | 1.44 |

## SHOCK-WAVE / TURBULENT BOUNDARY LAYER INTERACTION (SWTBLI)

We ran two simulations of shock-turbulent boundary layer interaction on two different grids: SWTBLI1 and SWTBLI2 (see Table 1). In both cases the shock is generated such that it impinges at $Re_\delta = 51,552$, $Ma = 2.25$ and under the angle $\beta = 33.2^\circ$, deflecting the mean flow by $\theta = 8^\circ$. The grid spacing is homogenous in streamwise and spanwise direction, while in wall-normal direction the points are clustered near the wall using a *tanh* function.

**Mean Flow Characterization** For high enough compression ratios, SWTBL interactions are characterized by boundary layer separation under the adverse pressure gradient imposed by the incident shock. The incoming flow is deflected upwards and compressed by the separated boundary layer and the compression waves form the "reflected shock" (the incident shockwave is actually reflected as an expansion fan). Further downstream a set of weak compression waves mark the boundary layer reattachment point (see Fig. 3). The separated boundary layer forms a shear layer on top of the reverse flow region. Its presence has an effect until far downstream of the average reattachment point and amplifies turbulent mass fluxes in a near-wall region. Turbulence amplification across this interaction can be observed in Fig. 4, where we plotted iso-surfaces of pressure, for showing the shocks, and of $\lambda_2 = -0.2$ colored by streamwise velocity to point out the turbulent structures existing in the boundary layer.

DNS of the same case have been performed by Pirozzoli and Grasso (2006) and Shahab and Gatski (2011). We compare skin friction coefficient and wall pressure distributions for our coarse and fine simulations with these DNS in Fig. 5. Fig. 5a shows the skin friction coefficient distribution averaged in spanwise direction and time. Differences have been found in calculating the $C_f$ from different viscosity laws. When using the powerlaw, we obtain $C_f \approx 0.002$ in the undisturbed boundary layer for both fine and coarse simulations. This powerlaw has been verified to be accurate in the previous TBL simulation. In both DNS simulations of the SWTBLI case, however, the friction coefficient has a slightly higher value. This is due to the use of Sutherland's law for viscosity in the DNS. When applying the corresponding correction to the DNS data, we are able to match the $C_f$ in the undisturbed TBL, as seen in Fig. 5a. For the recovering boundary layer we have a good agreement with the data from Shahab and Gatski (2011).

In Fig. 5b we plot the mean wall pressure over the di-

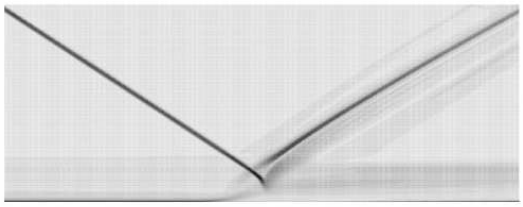

Figure 3. Numerical schlieren averaged in time and homogenous direction.

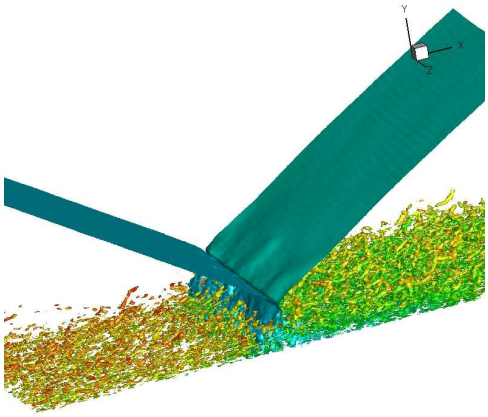

Figure 4. Instantaneous snapshot of shock-turbulent boundary layer interaction. Isosurfaces of pressure $p/p_0 = 0.22$ and $0.24$ and $\lambda_2 = -0.2$.

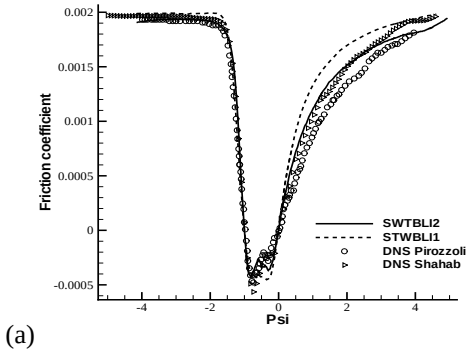


(a)

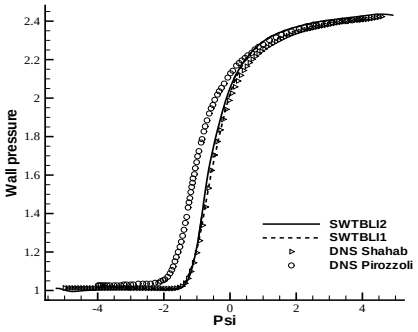


(b)

Figure 5. Averaged skin friction coefficient (a) and normalized wall pressure distribution (b).

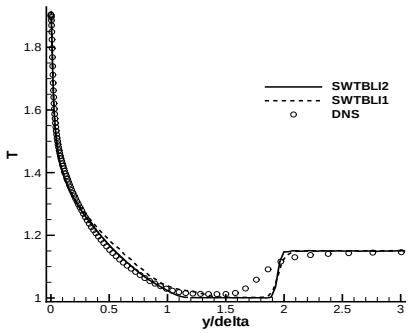


(a)

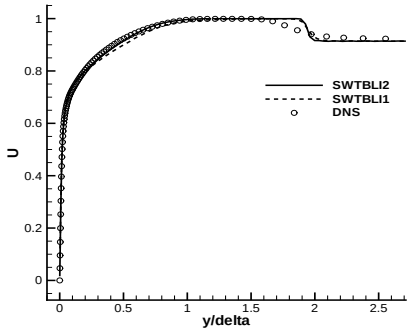


(b)

Figure 6. Mean temperature profiles (a) and mean velocity profiles (b) for DNS and LES.

mensionless coordinate $\Psi = (x - X_R)/(X_R - X_S)$, where $X_S$ is the spanwise and time averaged separation point and $X_R$ is the averaged reattachment point. Both our simulations agree very well with the DNS data of Shahab and Gatski (2011).The difference between our data and the DNS data from Pirozzoli and Grasso (2006) seems to come from an inconsistency of the computation of $\Psi$ for the DNS, since the separation bubble prediction is different in terms of $C_f$ and wall pressure.

We compared Favre-averaged temperature and Favre-averaged streamwise velocity at the location $Re_\delta \approx 50,000$ just upstream of the interaction. In both cases we observe a good agreement for the boundary layer profiles, see Fig. 6. It is interesting to note that the jump produced by the impinging shock in flow quantities is captured very accurately by our numerical scheme, proving ALDM performs well as turbulence model, while still being robust enough to capture shocks. Although employing a $7^{th}$ order WENO scheme for solving the inviscid fluxes, the DNS data shows a more smeared shock. This can be caused by poor resolution across the shock. Looking at the resolution in Y-direction in Pirozzoli's case, we observe that even if $\Delta y^+_{min} \approx 1$, there are only 111 points distributed across $6\delta_{Re=50,000}$, probably strongly clustered in the wall region. In our LES, we have for the coarse SWTBLI1 case, $\Delta y^+_{min} \approx 4$ with 177 points distributed over $5\delta$; and in the SWTBLI2 case, $\Delta y^+_{min} \approx 0.8$ with 198 points distributed over $5\delta$.

**Turbulence amplification** SWTBLI is characterized by the formation of a shear layer on top of the recirculation bubble. Fig. 7 shows a side view of the shear layer from our

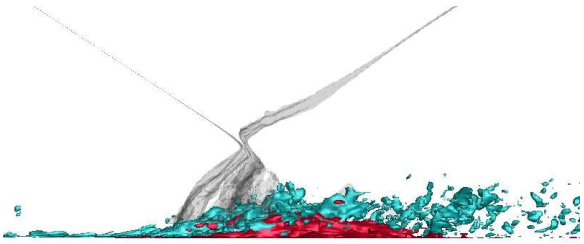

Figure 7. Side view of the shear layer produced in SWTBLI.

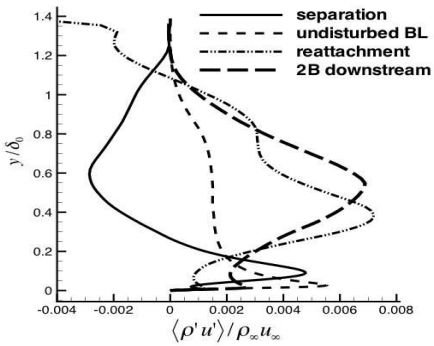


Figure 8. Streamwise turbulent mass flux at different streamwise locations.

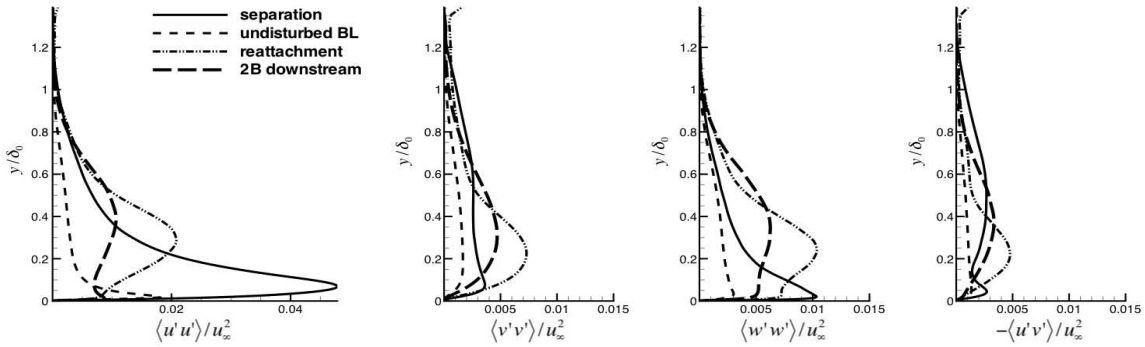


Figure 9. Reynolds stresses at different streamwise locations.

fine simulation. In grey we show the incident, respectively the reflected shock, represented by iso-surfaces of pressure at $p/p_\infty = 1.35$ and 1.63 respectively. The red iso-surfaces stand for the reverse flow region, while in light blue we show the wall-normal component of vorticity. The shear layer originates at the flow separation point and it persists throughout the rest of the computational domain, $18\delta_0$, locally amplifying turbulent mass fluxes. This phenomenon should be exploited in a SCRamjet combustor, because it can bring additional fuel/air mixing in the case of injectors positioned on the wall surface.

In Fig. 8 and 9 we show the evolution of the averaged turbulent mass fluxes and Reynolds stresses, respectively, in wall normal direction at relevant streamwise locations. The dashed lines represent quantities in the undisturbed TBL, while long dashes stand for a location situated at two bubble lengths downstream of the reattachment point. Continuous and dash dot dot curves denote quantities at separation, respectively reattachment point. The streamwise component $\langle \rho' u' \rangle$ of the turbulent mass fluxes increases by 36% over the interaction, while the absolute value of $\langle \rho' v' \rangle$ is three times larger than in the undisturbed TBL. The peak in both $\langle \rho' u' \rangle$ and $\langle \rho' v' \rangle$ moves away from the wall. The same trend is observed in the Reynolds stresses; they are amplified by a factor of three across the interaction, while their shape is altered.

**Shock motion** The reflected shock motion is recorded in the wall pressure signature. Given the expected low frequency characterizing the shock foot oscillation, we are looking at long computational times. This is on going work. Preliminary pressure spectra of the signal from the average separation point show a high low-frequency content in the range of 250-1000 Hz. This is in agreement with Priebe et al. (2009). However, the signal length in this reference is not large enough to conclude that the lowest computed frequency in the spectrum is also the lowest existent frequency in the signal. This is the reason why we are not referring to our results as final. In addition to the reflected shock motion, Priebe et al. (2009), as well as Loginov et al. (2006), have reported shocklet shedding after the interaction. This phenomenon is thought to be the source of turbulence amplification. In the present case we observe a similar formation of weak compression waves in the post-interaction region, but their life duration is short and no significant shedding of shocklets is observed.

## SHOCK-WAVE / TURBULENT BOUNDARY LAYER INTERACTION WITH HEAT ADDITION

The convection of an entropy spot (ES) through a shock results in baroclinic vorticity production and an acoustic wave. In a supersonic combustion engine, such as the SCRamjet, we have to deal with such flow situations: hotter regions, where fuel has burnt, or colder spots rich in unburnt fuel convecting through oblique shocks. In both cases vorticity is produced and this can enhance the turbulent mixing, leading to an improved engine efficiency. Hussaini and Erlebacher (1999) found that convecting a two-dimensional cold ES through a normal shock with the Mach number of $Ma = 2$ and 10 produces stronger maximum vorticity than a hot ES. In the case of an axisymetric ES however, the situation is reversed. An exhaustive investigation of shock/ES interaction for normal shock Mach numbers of $Ma = 2$ and 4 at three different weak ES amplitudes can be found at Fabre et al. (2001). The conclusion of the study was that the vorticity production in case of a cylindrical ES is far more important than in a case of an ES with Gaussian distribution of temperature. In the present study we consider a Gaussian distribution of density of the form $\rho = \rho_\infty \cdot (1 - \varepsilon \cdot e^{-r})$,where $\varepsilon$ is the ES amplitude and $r$ characterizes the radius. The pressure remains constant, the temperature profile follows the density distribution.

We conducted two simulations, one with maximum $\rho_{max} = 190\%\rho_\infty$ representing a cold ES, while the hot ES has a minimum density $\rho_{min} = 10\%\rho_\infty$. Both simulations were initialized with the solution from SWTBLI1 computation in which we inserted the density disturbance at a wall distance of approximately $2.5\delta$ and seven bubble lengths upstream of the separation point; the maximum, respectively the minimum density is located in the middle of the spanwise coordinate. Initial radius of the disturbance is $r = \delta_0$.

In order to estimate the effect of the temperature disturbance on turbulent mixing for both cold and hot entropy spots, we compare turbulent mass fluxes at the same time instant from two planes situated at spanwise coordinates $Z_1$ and $Z_2$ and two wall-normal locations, $Y_1 = 2.56\delta_0$ and $Y_2 = 3.14\delta_0$. We chose the $Z_1$ and $Z_2$ coordinates by estimating the spanwise vortex cores position of the pair of counter-rotating vortices. $Y_1$ and $Y_2$ are planes located outside of the boundary layer, which correspond to the position of maximum, respectively minimum, values of density at the time instant chosen for comparison. In Fig. 10 we present

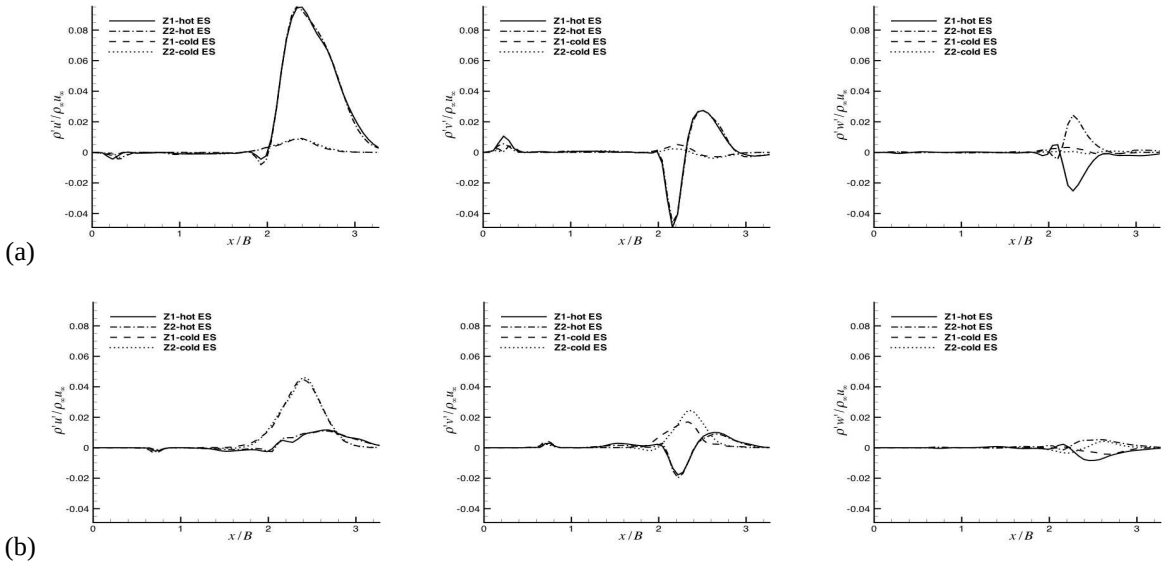


Figure 10. Turbulent massflux amplification at hot and cold ES convection through a shock (a) $Y_1 = 2.56\delta_0$ and (b) $Y_2 = 3.14\delta_0$.

the turbulent mass fluxes in $X-$, $Y-$ and $Z-$direction at the two different wall-normal coordinates as a function of the streamwise coordinate, normalized by the averaged bubble length, $B$. The dashed lines are results for a cold ES (higher density) and the continuous lines represent results for hot ES (lower density). The turbulent mass flux amplification has the same magnitude and sign for both $Z_1$ and $Z_2$ planes, for both hot and cold entropy spots. As expected, an exception from this is the spanwise mass flux, which follows the negative, respectively positive, spanwise velocity trend of the counter-rotating vortex pair. However, the magnitude of $\rho' w'$ stays the same for both $Z_1$ and $Z_2$ planes. In plane $Z_1$ there is maximum turbulence amplification for the hot ES, while in plane $Z_2$ for the cold ES. The magnitude of all three turbulent mass fluxes are almost two times larger in the case of a hot ES. Shortly after the ES hits the reflected oblique shock, we observed the formation of shocklets. These are however weak, and dissipate quite fast, not contributing significantly to turbulence amplification.

## CONCLUSION

We presented implicit LES of SWTBLI with and without heat addition at $Ma = 2.25$ and $Re_\delta = 51{,}552$. For the validation of our turbulence model, we ran a flat plate TBL simulation at the same free-stream parameters as in Pirozzoli et al. (2008). The results are in very good agreement with the DNS data. Also for the undisturbed SWTBLI simulations we matched mean profiles at a location before the interaction point with DNS data. Turbulence enhancement across the interaction was analyzed. The Reynolds stresses are amplified by a factor of up to three and their maximum moves away from the wall. No evidence for significant shocklet shedding in the wake of the reflected shock was found, unlike in the cases of other authors. We also investigated the effect of a Gaussian entropy disturbance applied to SWTBLI flow field. By looking at turbulent mass fluxes, we found that a hot ES would amplify turbulent mixing to a higher degree than a cold ES. Further research is devoted to periodic excitation.

## REFERENCES


Dussauge, J. P., Dupont, P., Debieve, J. F., 2006, "Unsteadiness in shockwave boundary layer interaction with separation", Aero. Science and Techn. Vol. 10, pp 85–91.

Fabre, D., Jacquin, L., Sesterhenn, J., August 2001, "Linear Interaction of a cylindrical entropy spot with a shock", Phys. of Fluids Vol. 13, Nr. 8, pp 2403–2422.

Hickel, S., Larsson, J., 2008, "An adaptive local deconvolution model for compressible turbulence". CTR Stanford Proc. Sum. Prog., pp. 85-96.

Hussaini, M. Y., Erlebacher, G., 1999, "Interaction of an Entropy Spot with a Shock", AIAA Journal, Vol. 37, Nr. 3, pp 346–356.

Loginov, M. S., Adams, N. A., Zheltovodov, A., 2006, "Large-eddy simulation of shockwave/turbulent-boundary-layer interaction", J. Fluid. Mech. Vol. 565, pp 135–169.

Pirozzoli, S., Bernardini, M. and Grasso, F., 2008, "Characterization of coherent vortical structures in a supersonic turbulent boundary layer", J. Fluid. Mech. Vol. 613, pp 205–231.

Pirozzoli, S., Grasso, F., 2006, "Direct numerical simulations of impinging shock wave/turbulent boundary layer interaction at Mach=2.25", Phys. of Fluids Vol. 18.

Priebe, S., Wu, M., Martin, P., May 2009, "Direct Numerical Simulation of a Reflected-Shock-Wave/Turbulent-Boundary-Layer Interaction", AIAA Journal Vol. 47, Nr. 5, pp 1173–1185.

Shahab., M. F. and Gatski, T., 2011, Private communication concerning DNS of shock-turbulent boundary layer Interaction at Mach = 2.25.

Touber, E., Sandham, N. D., 2008, "Oblique Shock Impinging on a Turbulent Boundary Layer: Low-Frequency Mechanisms", AIAA Journal, pp 4170.

Wu, M. and Martin, P. , 2008, "Analysis of the shock motion in shockwave and turbulent boundary layer interaction using direct numerical simulation data", J. Fluid. Mech. Vol. 594, pp 71–83.